ALKYLATED INDOLO[3,2,1-*JK*]CARBAZOLES AS NEW BUILDING BLOCKS FOR SOLUTION PROCESSABLE ORGANIC ELECTRONICS

Thomas Kader,*[a] Guangrong Jin,[b] Matthias Pletzer,[a] Dongge Ma,[b] Johannes Fröhlich,[a] Jiangshan Chen,*[b] and Paul Kautny [a]

[a] Institute of Applied Synthetic Chemistry, TU Wien, Getreidemarkt 9/163, A-1060 Vienna, Austria

[b] Institute of Polymer Optoelectronic Materials and Devices, State Key Laboratory of Luminescent Materials and Devices, South China University of Technology, Guangzhou, People's Republic of China

* thomas.kader@tuwien.ac.at, * msjschen@scut.edu.cn

Abstract

A facile strategy for the introduction of *tert*-butyl and hexyl chains to the indolo[3,2,1-*jk*]carbazole scaffold is presented. With these building blocks six materials based on three different 4,4'-bis(*N*-carbazolyl)-1,1'-biphenyl derivatives with varying degree of planarization were prepared. Characterization of the materials showed that the alkyl chains have only minor effects on the photophysical properties of the compounds. In contrast, thermal robustness towards decomposition and electrochemical stability are increased by the introduced alkyl chains. Detailed investigation of the solubility in five different solvents revealed that the incorporation of the alkyl chains increases the solubility significantly. The increased solubility of the materials allowed the application as host materials in red, green and blue solution processed PhOLEDs. Hence, this work presents the first solution processed OLED devices based on the indolo[3,2,1-*jk*]carbazole scaffold.

INTRODUCTION

Since the introduction of organic electroluminescent thin films,[1] followed by applications in first organic light emitting diodes (OLED) based on small molecules[2] and polymers,[3] functional organic materials for electroluminescent devices have been improved continuously. Especially the introduction of new light harvesting mechanisms like the use of transition metal emitters in phosphorescent OLEDs (PhOLEDs)[4, 5] and organic emitters using thermally activated delayed fluorescence (TADF)[6, 7] resulted in improved efficiencies. However, careful material design and device engineering is necessary to further improve device performance.

Recently, we investigated bipolar host materials using triarylamines with different degree of planarization, as donor subunits. Modification of the planarization allowed to control the intramolecular conjugation, as increasing planarization resulted in a decreased donor strength. Hence, the use of fully planarized indolo[3,2,1-*jk*]carbazole (ICz, molecular structure see chart 1, top, left) reduced intramolecular charge transfer and resulted in high triplet energies, as well as good thermal stability.[8] Besides its weakened donor strength, the versatility of the building block can be seen as itself has bipolar character[8-10] and can also be used solely as acceptor building block.[11, 12] Furthermore, the electronic properties can be tuned by incorporation of sulfur atoms to increase the donor strength,[13] as well as nitrogen incorporation[14] or substitution with cyano groups[15] to increase the acceptor strength.

Although ICz is known to literature for a long time,[16] it took quite long until first studies on conducting thin-films were executed.[17, 18] However, the development of more feasible synthetic approaches based on palladium catalyzed methodologies,[8, 19, 20] paved the way for the increased use of the ICz scaffold in organic electronics. In recent years the ICz scaffold became especially important as building block in dye sensitized[21-23] and perovskite solar cells,[24] and OLEDs. Particularly successful was the application of ICz as integral functional unit in host materials for PhOLEDs[8-10, 25-27] and TADF-OLEDs,[28] but also as building block for fluorescent[12, 27, 29, 30] and TADF emitters.[11, 12, 15] Additionally, the planar ICz motif was implemented in larger conjugated systems in electron donating molecules or materials employed as emitters.[30-34]

So far, all ICz based materials for OLED devices were exclusively processed by vacuum deposition. Besides the fact that small molecules are usually processed by vacuum deposition,[35] the planar and rigid backbone of ICz based materials causes low solubility which is usually not sufficiently high for solution processing techniques. With this work we aimed to further broaden the scope of the ICz building block by modifying the scaffold to increase its solubility and make it applicable for solution processing.

Despite some challenges, like the fabrication of multi-layered devices, there is an increasing interest in the fabrication of small molecule devices from solution, due to several advantages as milder conditions, faster processing and less material loss.[35-37]

However, beside several other factors adequate solubility in certain solvents remains as crucial factor for small molecules to be processed from solution. Our goal was to introduce alkyl chains to increase the solubility of the ICz building block and demonstrate the applicability of ICz based materials for solution processed OLEDs for the first time. In order to compare the effect of different alkyl chains we have chosen *tert*-butyl and *n*-hexyl as target groups that should be incorporated into the scaffold. While *tert*-butyl mono-substitution in position 2, double-substitution in positions 2 and 5 as well as trifold-substitution (2,5,11) are known in literature,[19] our goal was to achieve substitution in positions 5 and 11 to yield a symmetric building block (see chart 1).

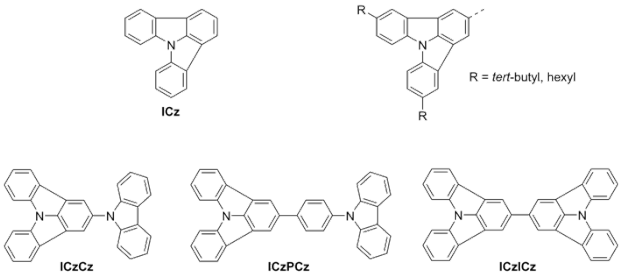

Chart 1. Structure of ICz (top, left), target alkyl substitution pattern of the ICz scaffold (top, right) and ICz based CBP-derivatives (bottom).

To get better insight on the effect of the alkyl chains on solubility and material properties we have chosen target materials based on the 4,4'-bis(*N*-carbazolyl)-1,1'-biphenyl (CBP) scaffold, that were already implemented as host materials for PhOLEDs (chart 1, bottom line).[9] Due to the different degree of planarization these materials have very diverse solubilities which allows for better comparison of the effect of alkylation. As further proof of concept, the new materials were used as host materials for solution processed PhOLED devices.

RESULTS AND DISCUSSION

Synthesis

The synthetic strategy towards the alkylation of the ICz building block is depicted in scheme 1 (left side, a). The *tert*-butyl substituted building block **2a** was synthesized in one step starting from the brominated ICz precursor **1** by Friedel Crafts alkylation using 2-chloro-2-methylpropane and $ZnCl_2$ as lewis acid in nitromethane. As substitution occurs exclusively in the desired positions para to the central nitrogen atom an excess of the alkylation reagent could be used yielding **2a** almost

quantitatively. Introduction of the hexyl chains was achieved in a similar approach employing first a Friedel-Crafts acylation with hexanoyl chloride and $AlCl_3$ as lewis acid. Subsequently, the carbonyl groups were reduced with $LiAlH_4$ giving the hexyl building block **2c** with an excellent yield of 80% over both steps. Finally, the halogenated precursors were converted to the corresponding boronic acid esters by Miyaura borylation, to prepare the precursors required for Suzuki cross coupling. Using standard conditions with $PdCl_2$(dppf) and KOAc as base, **3a** and **3b** were obtained in good yields of 70% and 71%, respectively. Furthermore, for the synthesis of the CBP derivatives the alkylated carbazole and phenylcarbazole species were required. Alkylation of 9*H*-carbazole was achieved according to literature procedures.[38, 39] While **5b** is not known to peer-reviewed literature it can be prepared in the same way as **5a** by a nucleophilic substitution of 1-bromo-4-fluorobenzene with the alkylated carbazole using Cs_2CO_3 as base.[40] Analogously to the ICz building blocks, **6a** and **6b** were converted to the boronic acid ester species by Miyaura borylation.[41]

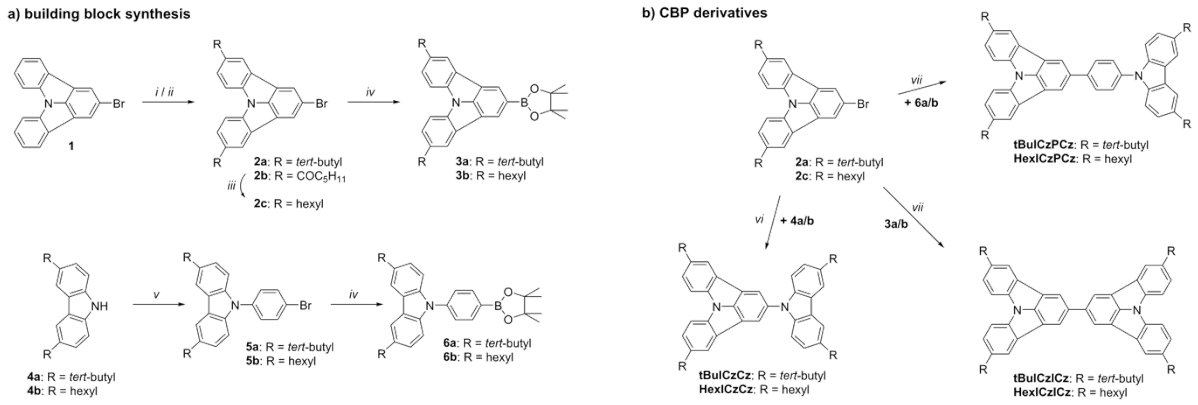

Scheme 1. Synthetic approach towards alkylation of **1** and synthesis of target materials **RICzCz**, **RICzPCz** and **RICzICz** (R = *tert*-butyl, hexyl). Reaction conditions: *i*: 2-chloro-2-methylpropane, $ZnCl_2$, CH_3NO_2, 0 °C – rt; *ii*: hexanoyl chloride, $AlCl_3$, CH_2Cl_2, 0 °C – rt; *iii*: $LiAlH_4$, $AlCl_3$, Et_2O, CH_2Cl_2, 0 °C – rt; *iv*: bis(pinacolato)diboron, KOAc, $PdCl_2$(dppf)*CH_2Cl_2, DMF, 100 °C; *v*: 1-bromo-4-fluorobenzene, Cs_2CO_3, DMF, 150 °C; *vi*: K_2CO_3, $CuSO_4$*$5H_2O$, 230 °C; *vii*: K_2CO_3 (2M in H_2O), $Pd(PPh_3)_4$, THF, reflux.

With all the alkylated building blocks in hand the target materials **RICzCz**, **RICzPCz** and **RICzICz** (R= *tert*-butyl or hexyl) could be synthesized (scheme 1 right, b). C-N bond formation of the carbazole based materials was accomplished by Ullmann condensation of the halogenated ICz building block with the corresponding carbazole. A solvent free reaction protocol using $CuSO_4$*$5H_2O$ and K_2CO_3 at 230 °C yielded **tBuICzCz** and **HexICzCz** with 77% and 78% yield, respectively. The remaining materials were synthesized by Suzuki coupling using $Pd(PPh_3)_4$ with aqueous K_2CO_3 as base in THF with yields ranging from 35% to 74%. All intermediates and target materials were characterized by ^1H and ^{13}C NMR spectroscopy as well as high-resolution mass spectrometry.

Solubility

The effect of the introduction of alkyl chains on the solubility of the materials at room temperature was determined in chloroform, isopropanol, *n*-hexane, tetrahydrofuran and toluene by absorption spectroscopy. The results of these experiments are summarized in table 1. A graphical comparison of the solubility in chloroform is depicted in figure 1.

Table 1. Solubility in mg/ml of the CBP-derivatives at 22 °C in different solvents. Average values including standard deviation of three experiments are given.

	solvent	R = H	R = *tert*-butyl	R = *n*-hexyl
RICzCz	$CHCl_3$	58.1±3.1	308.9±12.3	564.9±10.4
	iPrOH	0.08±0.003	2.6±0.2	0.6±0.01
	n-hexane	0.18±0.005	19.8±2.5	335.6±17.9
	THF	79.4±1.7	182.7±5.6	663.7±47.7
	toluene	22.1±0.5	278.7±10.8	610.3±39.2
RICzPCz	$CHCl_3$	23.9±1	302.7±0.8	448.5±17
	iPrOH	0.03±0.002	0.07±0.002	0.04±0.006
	n-hexane	0.04±0.003	2±0.03	6.5±0.7
	THF	35.9±1.6	229.8±15.7	378.7±1.6
	toluene	6.8±0.1	112.3±10.3	205.6±3.9
RICzICz	$CHCl_3$	1.8±0.02	12.5±1.5	92±2.1
	iPrOH	ins.[a]	0.05±0.001	0.04±0.003
	n-hexane	ins.[a]	0.36±0.02	0.83±0.03
	THF	3.6±0.09	12±0.5	80±6.3
	toluene	0.65±0.01	5.2±0.2	40.2±3.1

[a] insoluble (solubility <0.01 mg/ml)

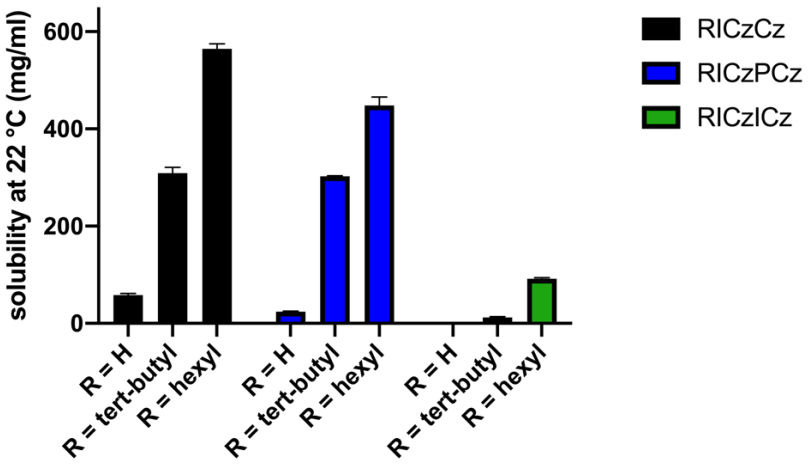

Figure 1. Comparison of the solubility in mg/ml of **RICzCz** (left), **RICzPCz** (middle) and **RICzICz** (right) derivatives in chloroform at room temperature.

As expected, the solubility of the materials decreases with increasing planarization from **ICzCz** to **ICzICz**. Notably, **ICzICz** has a very low solubility with a maximum solubility of 4 mg/ml in THF. As envisioned, the introduction of the alkyl chains leads to a significant increase in solubility. For hexyl substituted compounds a higher solubility is observed compared to *tert*-butyl groups, with exception of iPrOH, in which however the materials remain rather insoluble, independent of the nature of the substituent R. Especially **HexICzCz** shows exceptional high solubility in all solvents except iPrOH. Even the solubility of the worst soluble hexyl based derivative **HexICzICz** is nearly doubled in chloroform and toluene, compared to the best soluble non-alkylated derivative **ICzCz**. The non-alkylated materials are best soluble in THF, followed by chloroform and toluene. In contrast, this trend is overturned for the alkylated derivatives which have their highest solubility in chloroform. Nevertheless, except for **tBuICzICz**, which shows only moderate solubility, despite a significant increase compared to **ICzICz**, all other materials show good solubility, suitable for solution processing.

Photophysical properties

UV/vis absorption and fluorescence spectra, as well as low temperature photoluminescence spectra were recorded to determine the effect of alkylation on the photophysical properties of the new materials and for comparison with the non-alkylated materials (figure 2 and 3, table 2). Substitution with alkyl chains causes a slight shift of the lowest energy absorption peak to higher wavelengths in the order H<*tert*-butyl<hexyl. The optical gap of the carbazole based materials (**RICzCz**) is slightly lower compared to **RICzPCz** and **RICzICz**. Therefore, **tBuICzCz** and **HexICzCz** show the smallest optical gaps with 3.05 eV and 3.03 eV, respectively, while **ICzPCz** and **ICzICz** feature the largest (3.20 eV). Moreover, all materials show a distinct absorption peak between 286 nm and 292 nm that can be attributed to the π - π* transitions of the materials.[9] In analogy to the absorption onset, these peaks are slightly redshifted in the case of alkylated **RICzCz** and **RICzPCz**. For **ICzCz** and **ICzPCz** a shoulder at higher wavelength is observed close to these peaks, which appears as distinct peak at 300 nm in the case of the alkylated species. In contrast this feature cannot be found for **RICzICz** derivatives.

Analogously, the emission maxima of the fluorescence spectra of the **RICzCz** and **RICzPCz** derivatives, are shifted to higher wavelengths. Notably, hexyl substituents induce a slightly more pronounced shift compared to *tert*-butyl. In contrast, the emission maxima of **tBuICzICz** and **HexICzICz** are not shifted compared to the non-alkylated material.

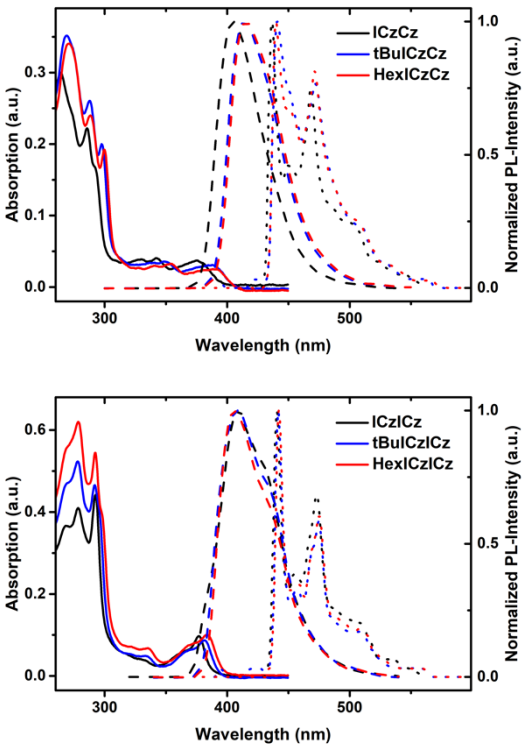

Figure 2. UV/Vis absorption (full lines), normalized fluorescence (dashed lines) and normalized low temperature phosphorescence spectra (dotted lines) of **RICzCz** (top, left), **RICzPCz** (top, right) and **RICzICz** (bottom, left) derivatives. Absorption and fluorescence spectra recorded in CH_2Cl_2 (5 µm) at room temperature; phosphorescence spectra recorded at 77 K as solid solutions in 9:1 toluene:ethanol (0.5 mg/ml).

Table 2. Physical data of the investigated materials.

		Opt. Gap [eV][a]	λ_{max} [nm]	E_T [eV][b]	HOMO/ LUMO [eV][c]	$T_g/T_{rc}/T_m/T_d$ [°C][d]
RICzCz	R = H	3.14	405	2.84	-5.56 /-2.42	111/156/253/344
	R = *tert*-butyl	3.05	415	2.81	-5.40/-2.35	190/255/294/456
	R = hexyl	3.03	416	2.82	-5.42/-2.39	n.o.[e]/n.o.[e]/91/456
RICzPCz	R = H	3.20	386	2.83	-5.56 /-2.36	119/165/262/385
	R = *tert*-butyl	3.13	396	2.82	-5.45 /-2.32	197/266/356/486
	R = hexyl	3.11	399	2.82	-5.44 /-2.33	84/n.o.[e]/112/458
RICzICz	R = H	3.20	409	2.81	-5.39 /-2.19	n.o.[e]/n.o.[e]/383/408
	R = *tert*-butyl	3.15	409	2.81	-5.44 /-2.29	n.o.[e]/n.o.[e]/n.o.[e]/499
	R = hexyl	3.13	406	2.81	-5.38 /-2.25	113/n.o.[e]/314/461

[a] Determined from absorption onset. [b] Estimated from the highest energy vibronic transition in solid solutions of toluene/EtOH (9:1) at 77 K. [c] HOMO levels were calculated from the onset of the oxidation peak. CV-measurements were carried out in a 0.5 mM solution in anhydrous DCM with Bu_4NBF_4 (0.1 M) as supporting electrolyte; LUMO levels were calculated from HOMO levels and the optical gap. [d] T_g: glass transition temperature. T_{rc}: recrysatllization temperature. T_m: melting point. T_d: decomposition temperature (5% weight loss in TGA analysis). [e] Not observed.

In order to determine the triplet energies of the materials, low temperature phosphorescence spectra were recorded at 77 K. Compared to the room temperature fluorescence all materials exhibit vibronically resolved spectra. Except of **tBuICzCz** and **HexICzCz** which show a more intense redshifted shoulder at the highest energy transition compared to **ICzCz**, the spectra of all other alkylated materials exhibit a very similar shape compared to their parent derivatives. In analogy to the

fluorescence spectra, the phosphorescence spectra of the alkylated derivatives of **RICzCz** and **RICzPCz** are slightly redshifted compared to **ICzCz** and **ICzPCz**, albeit the shift is less pronounced compared to the fluorescence spectra. Again, such a redshift is absent in the **RICzICz** series. Moreover, all alkylated materials retain high triplet energies >2.81 eV, which makes them applicable as host materials in blue PhOLED devices.

Electrochemical properties

The HOMO energy levels of the materials were estimated from the onset of the oxidation peaks obtained during cyclic voltammetry measurements. LUMO energy levels were calculated from the HOMO levels and the optical gaps determined by UV/Vis absorption spectroscopy. The results are summarized in table 2.

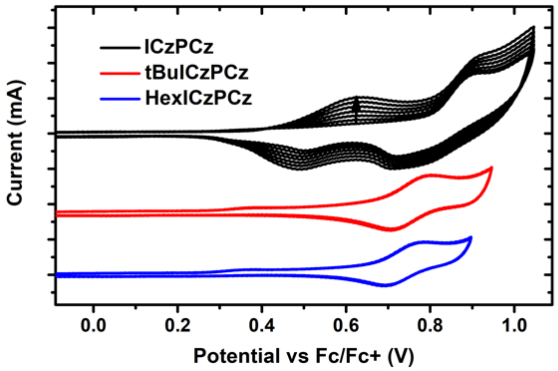

Figure 3. CV curves of 7 consecutive oxidation runs of **RICzPCz** derivatives in CH_2Cl_2 using Bu_4NBF_4 as electrolyte.

In the case of **RICzCz** and **RICzPCz** alkylation leads to an increase of the HOMO energy levels of roughly 0.15 eV and 0.11 eV, respectively compared to the non-alkylated materials (-5.56 eV). Due to the reduced optical gaps of the alkylated materials the LUMO levels are increased to a smaller extent. In contrast, in the case of the **RICzICz** derivatives, the introduction of hexyl chains showed no significant effect on the energetic location of the HOMOs. Caused by the smaller optical gap the alkylated materials of the **RICzICz** series have slightly lower LUMO levels.

Furthermore, the alkylated materials show reversible oxidation (consecutive oxidation runs depicted in figure 3 and supporting information figures S2 and S3). For indolo[3,2,1-*jk*]carbazole,[17] as well as carbazole[42, 43] based materials the high reactivity of the radical cationic species which is formed during oxidation, leads to formation of oligomeric species which are coupled via the para position of the nitrogen. This oligomerization can be observed by the formation of films on the electrodes.[17] Therefore, the incorporation of alkyl chains in these para positions increases the electrochemical

stability of the materials making the oxidation reversible over several scans, without any electrochemical indication dimerization or polymerization and without the formation of thin films.

Thermal properties

Thermal properties were investigated by STA to determine the effect of the alkyl chains on the thermal stability of the materials. TGA and DSC curves can be found in the supporting information, the determined values are summarized in table 2. In general, all materials show the same trend of an increase of all phase transitions and decomposition temperatures with increasing planarization of the scaffold, from **RICzCz** to **RICzPCz** and **RICzICz**. More differentiated observations were made regarding the effect of the alkylation. TGA analysis of the materials revealed that the thermal stability towards degradation was significantly increased by incorporation of alkyl chains. All alkylated materials begin to decompose only above 450 °C, almost 50 °C higher than **ICzICz**, which is the most stable of the non-alkylated reference materials. Especially **tBuICzPCz** and **tBuICzICz** show no thermal degradation until approximately 500 °C.

A different situation can be found for glass transition temperature (T_g) and melting points (T_m). In the case of incorporation of the *tert*-butyl groups both T_g and T_m are increased significantly and are higher than 190 °C and 294 °C respectively. In contrast, the incorporation of hexyl chains leads to a lowering of glass transitions temperatures and melting points. Interestingly, **HexICzCz** and **HexICzPCz** show only clear melting points during the first heating cycle, while no distinct signal can be found in the 2nd cycle. This indicates that these don't solidify again after the first cycle.

OLED devices

The developed materials were evaluated as universal host materials for RGB PhOLED devices, to investigate the applicability of the alkylated ICz scaffold for solution processing. **tBuICzCz** (**I**), **tBuICzPCz** (**II**), **HexICzCz** (**III**) and **HexICzPCz** (**IV**) were successfully employed. In contrast, **tBuICzICz** was not soluble enough to be used for solution processed devices. Although **HexICzICz** exhibits sufficient solubility, in initial experiments only poor device performance was observed. Therefore, this material was not considered for the devices presented in this work. Due to the high E_Ts of the materials Ir(MDQ)$_2$(acac) (**R**), Ir(ppy)$_2$(acac) (**G**) and FIrpic (**B**) were used as dopants. The PhOLED devices were fabricated using a standard device architecture of ITO/PEDOT:PSS (40 nm)/PVK (30 nm)/EML (50 nm)/TPBi or TmPyPB (40 nm)/LiF (1 nm)/Al. PEDOT:PSS and LiF were used as hole and electron injection layer, respectively. PVK was used as hole transport layer, while TPBi for red and green devices and TmPyPB for blue devices were employed as electron transport layer. The ICz based host materials with the corresponding phosphorescent emitters were used with a doping concentration of 10%.

Current density-voltage-luminance and current efficiency-luminance-power efficiency curves of the devices are depicted in figure 4. External quantum efficiency-luminance curves and

photoluminescence spectra of the devices can be found in the supporting information. The key electroluminescent properties of the devices are summarized in table 3.

Within the red device series (**RI-RIV**), devices employing host materials based on the **ICzPCz** scaffold exhibit better device performance in terms of efficiency, compared to those based on **ICzCz**. While this increase is only weakly pronounced for the *tert*-butyl substituted materials, the maximum current efficiency (*CE*) is increased to 10.12 cd/A, the maximum power efficiency (*PE*) to 3.13 lm/W and the maximum external quantum efficiency (EQE) to 6.5% for **RIV**, compared to **RIII** (*CE*: 3.57 cd/A, *PE*: 1.26 lm/W, EQE: 2.3%). The direct comparison of the different alkyl chains of the host materials reveals that the efficiency is significantly increased for the hexyl derivative **HexICzPCz** in **RIV**, compared to its *tert*-butyl analogue in **RII**, while nearly no difference is observed for the **ICzCz** scaffold in **RI** and **RIII**. Additionally, also the turn-on voltage (V_{ON}) is decreased from 9.4 V and 8.4 V in **RI** and **RII**, respectively, to 7.4 V using the hexyl based host materials. However, for **RIII** and **RIV** containing the hexyl based materials a lower maximum brightness and increased efficiency roll-off was observed. Furthermore, the electroluminescence spectra reveal minor emission from the host materials. These findings indicate poor film formation in these samples. However, in devices **RI** and **RII** emission is exclusively observed from the dopant, indicating efficient energy transfer from the host material to the emitter.

Analogously, for the devices with the green dopant (**GI-GIV**) improved device performance is observed for phenylcarbazole based materials **RICzPCz** in direct comparison with the corresponding carbazole derivatives. For **tBuICzPCz** the maximum *CE* and *PE* are almost doubled to 8.10 cd/A and 2.12 lm/W, compared to **tBuICzCz**, while remaining an onset voltage (V_{ON}) of 8.0 V. Notably, both hexyl based materials exhibit better overall device performance compared to the *tert*-butyl substituted compounds. Also, in this case **HexICzPCz** yields the best operating device with a *CE* of 19.62 cd/A and a *PE* of 9.40 lm/W resulting in 5.5% external quantum efficiency. In contrast to the red emitters, also the brightness is increased using the hexyl substituted host materials and no emission from the host materials is detected.

The performance of devices employing the blue dopant follows the trends observed for the red emitters. Similar performance with V_{ON} between 6.2 V and 6.8 V, *CE* and *PE* of about 4.5 cd/A and 1.75 lm/W, respectively can be detected for **BI-BIII** using **tBuICzCz**, **tBuICzPCz** or **HexICzCz**. In comparison, employing **HexICzPCz** (**BIV**) results in superior device performance with a lower V_{ON} of 5.4 V and a higher *CE* and *PE* of 9.55 cd/A and 5.04 lm/W, respectively. Similar to the red devices, increased efficiency roll-off, lower brightness and minor host emission can be observed for the hexyl based host materials in **BIII** and **BIV**.

In summary, employing the hexyl substituted host materials resulted in higher efficiency of the devices, compared to the *tert*-butyl substituted materials. Notably, employing **HexICzPCz** in **RIV**, **GIV**

and **BIV**, yielded the best performance within each series. However, in the case of red and blue devices the hexyl substitution resulted in lower brightness and high efficiency roll-off, which might be attributed to varying film formation of the different alkyl chains.

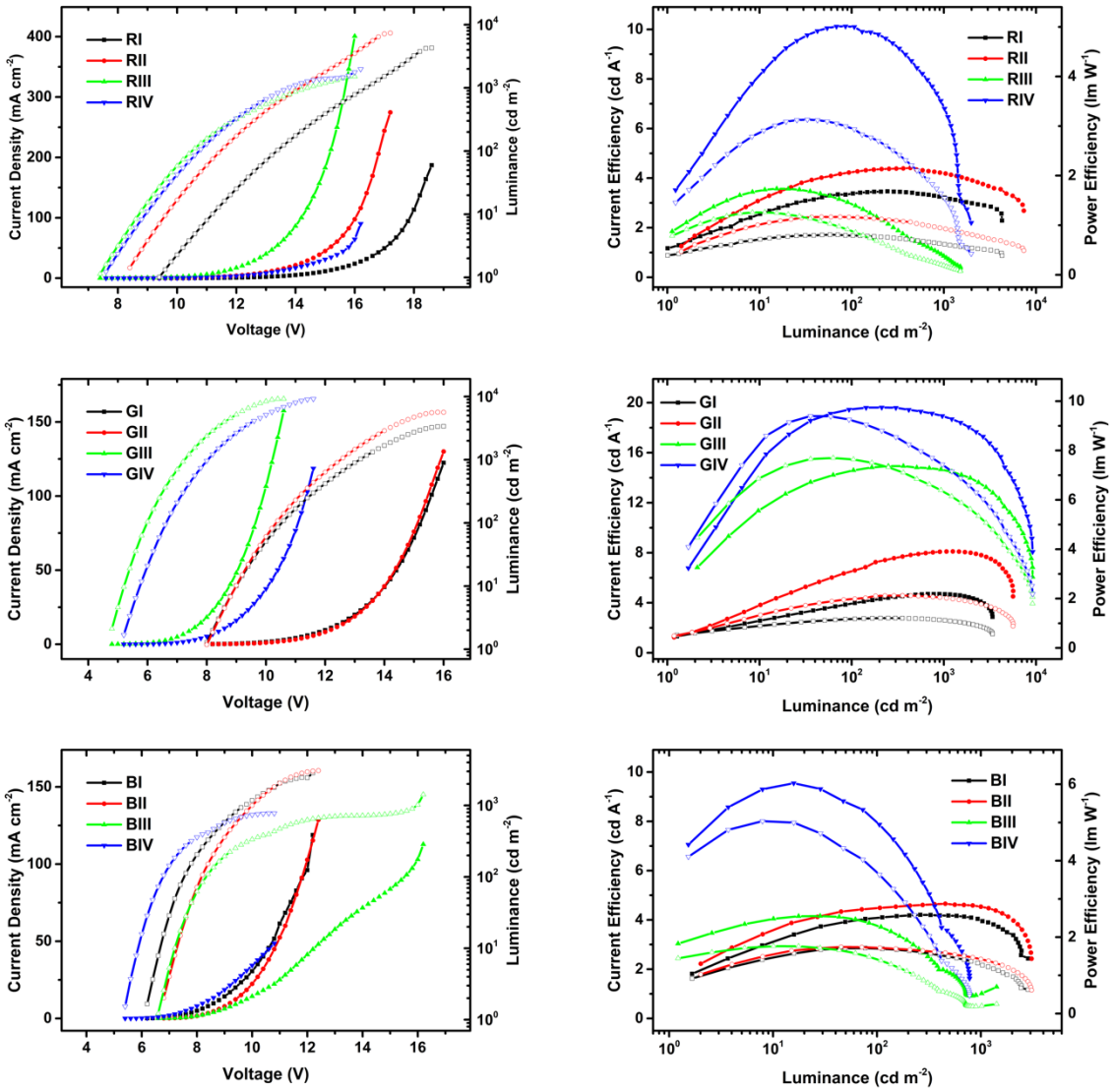

Figure 4. Current density-voltage-luminance (left; current density: solid symbols, luminance: hollow symbols) and current efficiency-luminance-power efficiency (right; current efficiency: solid symbols, power efficiency: hollow symbols) curves of $Ir(MDQ)_2(acac)$ red (top row), $Ir(ppy)_2(acac)$ green (middle row) and FIrpic based blue (bottom row) device. The corresponding dopants were dispersed with a concentration of 10% in **tBuICzCz** (**I**), **tBuICzPCz** (**II**), **HexICzCz** (**III**) and **HexICzPCz** (**IV**) as host materials.

Table 3. Performance of fabricated PhOLED devices.

Dopant	Device	Host	V_{ON} [V][a]	L [cd/m^2][b]	CE [cd/A][c]	PE [lm/W][d]	EQE [%][e]
Ir(MDQ)$_2$(acac) (red)	**RI**	**tBuICzCz**	9.4	4283	3.47	0.81	2.11
	RII	**tBuICzPCz**	8.4	7381	4.41	1.17	2.79
	RIII	**HexICzCz**	7.4	1509	3.57	1.26	2.26
	RIV	**HexICzPCz**	7.6	1985	10.12	3.13	6.52
Ir(ppy)$_2$(acac) (green)	**GI**	**tBuICzCz**	8.0	3379	4.70	1.21	1.33
	GII	**tBuICzPCz**	8.0	5631	8.10	2.12	2.26
	GIII	**HexICzCz**	4.8	9181	14.93	7.70	4.18
	GIV	**HexICzPCz**	5.2	9194	19.62	9.40	5.45
FIrpic (blue)	**BI**	**tBuICzCz**	6.2	2850	4.21	1.71	2.34
	BII	**tBuICzPCz**	6.8	3077	4.66	1.75	2.53
	BIII	**HexICzCz**	6.6	1418	4.15	1.76	2.26
	BIV	**HexICzPCz**	5.4	778	9.55	5.04	4.90

[a] Turn-on voltage at 1 cd/m^2. [b] Maximum luminance. [c] Maximum current efficiency. [d] Maximum power efficiency. [e] Maximum external quantum efficiency.

CONCLUSIONS

We developed a reliable, easy and high yielding synthetic approach for the introduction of *tert*-butyl and hexyl chains into the ICz building block that can be easily upscaled to multi-gram synthesis. To investigate the effect of the alkyl chains in detail six CBP derivatives with different degree of planarization were synthesized. Notably, the overall solubility of the alkylated materials significantly improved compared to the non-alkylated materials. Among the investigated alkyl chains hexyl provided a better solubility compared to *tert*-butyl. Furthermore, the alkyl chains improved the electrochemical stability of the materials, due to the prevention of oligomerization, as well as the thermal stability towards decomposition. In contrast, the alkyl chains have only minor impact on the absorption onset and fluorescent emission and high triplet energies are retained in the alkylated materials. Thus, the concept of solubility improvement by the introduction of alkyl chains without the deterioration of the desired photophysical and electrochemical properties of the parent materials was successfully executed for this class of compounds. Four of the materials were used as host materials in red, green and blue solution processed PhOLEDs, to demonstrate the ability of the alkylated building blocks to facilitate solution processing of devices and prove the practical applicability of the developed building blocks.

EXPERIMENTAL SECTION

All solvents and reagents were obtained commercially and used without further purification. Zinc chloride was dried by melting under vacuum prior to use. Anhydrous solvents were prepared by filtration through drying columns. Column chromatography was performed on silica 60 (Merck, 40-63 µm). Prior to device fabrication, all materials were purified by subsequent refluxing and filtration after cooling in *tert*-butanol, isopropanol and acetonitrile.

Absorption and photoluminescence measurements were conducted using a Thermo Scientific NanoDrop One^{C} UV-Vis spectrophotometer and a PerkinElmer LS 55 fluorescence spectrometer, respectively. CH_2Cl_2 solutions (5 µM) were employed for solution measurements while phosphorescence spectra were recorded at 77 K using solid solutions of the materials in toluene/EtOH (9/1; 0.5 mg/ml) with a delay of 1 ms. Cyclic voltammetry was measured using a three electrode configuration consisting of a Pt working electrode, a Pt counter electrode, and an Ag/AgCl reference electrode and a PGSTAT128N potentiostat provided by Metrohm Autolab B.V. The measurements were carried out in a 0.5 mM solution in CH_2Cl_2 employing Bu_4NBF_4 (0.1 M) as supporting electrolyte. Prior to the measurements, the solutions were purged with nitrogen for approximately 15 minutes. The HOMO energy levels were calculated from the onset of the oxidation peaks. LUMO energy levels were calculated from the HOMO levels and the optical gap. The onset potential was determined by the intersection of two tangents drawn at the background and the rising of the oxidation peaks. Simultaneous Thermal Analysis (STA) was performed on a Netsch STA 449 F1 using Al pans with a heating rate of 10 K/min und nitrogen atmosphere. Nuclear magnetic resonance (NMR) spectra were recorded on a Bruker Avance III HD 600 MHz spectrometer equipped with a cryo probe Prodigy™ at 600.2 MHz (^{1}H) and 150.9 MHz (^{13}C). The chemical shifts are reported in δ units, parts per million (ppm) downfield from tetramethylsilane using residual solvent signals for calibration. Coupling constants are reported in Hertz; multiplicity of signals is indicated by using following abbreviations: s=singlet, d=doublet, t=triplet, q=quartet, quint=quintet and m=multiplet. High resolution mass spectra (HRMS) (m/z 50-1900) were obtained on a maXis UHR ESI-Qq-TOF mass spectrometer (Bruker Daltonics, Bremen, Germany) in the positive-ion mode by direct infusion. The sum formulas of the detected ions were determined using Bruker Compass DataAnalysis 4.1 based on the mass accuracy ($\Delta m/z \leq 5$ ppm) and isotopic pattern matching (SmartFormula algorithm).

Device fabrication

The devices were fabricated on clean glass substrates precoated with an indium tin oxide (ITO) layer (185 nm) with a sheet resistance of 8 Ω per square. The ITO surface was treated in an ultrasonic detergent bath for 90 min, soaked in ultrasonic de-ionized water for 20 min, then dried at 120 °C for 1 h, and cleaned with UV/Ozone for 15 min before spin coating. A PEDOT:PSS layer (40 nm) was spin-

coated onto the ITO surface at 3000 rpm, then baked at 150 °C for 30 min to remove the residual water. Subsequently, the PVK layer was spincoated onto the PEDOT:PSS layer at 2500 rpm from a filtered 10 mg/mL chlorobenzene solution, and then dried at 120 °C for 20 min. Following that, the emitting layer was spin-coated according to the configuration requirement. Solutions of $Ir(MDQ)_2acac$, $Ir(ppy)_2$ or FIrPic (10 wt%) doped in the corresponding ICz based host material with a total concentration of 15 mg/ml in chlorobenzene were spin-coated at 1500 rpm for 30 s. Finally, an electron-transport layer TPBi or TmPyPB, a LiF layer, and an Al layer were deposited consecutively onto the spin-coated film in a vacuum chamber at 10^{-4} Pa. The emission area of the device was 4×4 mm^2, as shaped by the overlapping area of the anode and cathode. All the device characterization steps were carried out at room temperature under ambient laboratory conditions without encapsulation. EL spectra were recorded by an optical analyzer, Flame-S-VIS-NIR. Current density and luminance versus driving voltage characteristics were measured by a Keithley 2400 and a Konica Minolta chromameter CS-200. External quantum efficiencies were calculated by assuming that the devices were Lambertian light sources.

Synthetic details

2-Bromoindolo[3,2,1-*jk*]carbazole (**1**),[8] 3,6-bis(1,1-dimethylethyl)-9*H*-carbazole (**4a**),[38] 3,6-dihexyl-9*H*-carbazole (**4b**),[39] 9-(4-bromophenyl)-3,6-bis(1,1-dimethylethyl)-9*H*-carbazole (**5a**),[40] and 3,6-bis(1,1-dimethylethyl)-9-(4-(4,4,5,5-tetramethyl-1,3,2-dioxaborolan-2-yl)phenyl)-9*H*-carbazole (**6a**)[41] were prepared according to literature.

9-(4-Bromophenyl)-3,6-dihexyl-9*H*-carbazole (5b). 3,6-Dihexyl-9*H*-carbazole (1.68 g, 5 mmol) and Cs_2CO_3 (6.52 g, 20 mmol) were added to a three-neck flask. 20 ml DMF and 1-bromo-4-fluorobenzene (3.51 g, 20 mmol) were added and mixture was heated to 150 °C. After 24 h additional 1-bromo-4-fluorobenzene (1.75 g, 10 mmol) was added and the reaction mixture was heated for further 16 h. The mixture was then cooled to room temperature and poured into water and repeatedly extracted with CH_2Cl_2. The combined organic phases were dried over anhydrous Na_2SO_4 and concentrated under reduced pressure. The crude product was purified by column chromatography (light petroleum) yielding **5b** as colorless oil (2.19 g, 4.46 mmol, 89%) which crystallized after several days. ^{1}H NMR (600 MHz, CD_2Cl_2) δ 7.92 (s, 2H), 7.72 (d, J = 8.6 Hz, 2H), 7.46 (d, J = 8.6 Hz, 2H), 7.30 (d, J = 8.3 Hz, 2H), 7.23 (d, J = 9.7 Hz, 2H), 2.79 (t, J = 7.6 Hz, 4H), 1.72 (p, J = 7.6 Hz, 4H), 1.44 – 1.31 (m, 12H), 0.91 (t, J = 7.0 Hz, 6H). ^{13}C NMR (151 MHz, CD_2Cl_2) δ 139.7, 137.9, 135.5, 133.5, 128.9, 127.2, 124.1, 120.7, 120.1, 109.7, 36.5, 32.9, 32.4, 29.6, 23.2, 14.5. HRMS (ESI): m/z calculated for $C_{30}H_{37}BrN^+$ $[M+H]^+$ 490.2104, found 490.2106.

2-Bromo-5,11-bis(1,1-dimethylethyl)-indolo[3,2,1-*jk*]carbazole (2a). $ZnCl_2$ (15.25 g, 111.9 mmol) and 2-bromoindolo[3,2,1-*jk*]carbazole (9.84 g, 30.73 mmol) were added to a dried three-neck flask and flushed with argon. After addition of 90 ml CH_3NO_2 the reaction was cooled with ice/water and 2-chloro-2-methylpropane (9.96 g, 107.6 mmol) was added dropwise. The reaction mixture was slowly warmed to room temperature and stirred overnight. The reaction was poured into cooled water and repeatedly extracted with $CHCl_3$. The combined organic phases were washed with brine, dried over anhydrous Na_2SO_4 and concentrated under reduced pressure. The crude product was flashed over silica (CH_2Cl_2) yielding **2a** (12.94 g, 29.93 mmol, 97%) as off-white solid. ^{1}H NMR (600 MHz, $CDCl_3$) δ 8.14 (s, 2H), 8.08 (d, J = 1.9 Hz, 2H), 7.75 (d, J = 8.5 Hz, 2H), 7.61 (dd, J = 8.5, 1.9 Hz, 2H), 1.47 (s, 18H). ^{13}C NMR (151 MHz, $CDCl_3$) δ 145.2, 142.8, 137.1, 129.1, 125.1, 122.2, 120.0, 115.6, 111.6, 35.0, 32.0. HRMS (ESI): m/z calculated for $C_{26}H_{26}BrN^+$ $[M]^+$ 431.1243, found 431.1248.

1,1'-(2-Bromoindolo[3,2,1-*jk*]carbazole-5,11-diyl)bis(hexan-1-one) (2b). $AlCl_3$ (8.39, 62.9 mmol) was added to a dry three-neck flask and flushed with argon. After the addition of 65 ml anhydrous CH_2Cl_2 the reaction was cooled with ice/water. Hexanoyl chloride (8.49 g, 63.1 mmol) was added and the reaction mixture was stirred for 10 min. Subsequently, 2-bromoindolo[3,2,1-*jk*]carbazole (**1**) (8.10 g, 25.3 mmol) was added under argon counterflow. The reaction mixture was slowly warmed to room temperature and stirred overnight. About half of the solvent was evaporated under reduced pressure and the remaining solution was poured into ice/water. The resulting precipitate was filtered off and washed with 2N NaOH, water and methanol. After drying the crude product was refluxed in acetonitrile and filtered subsequently yielding **2b** (12.01 g, 23.3 mmol, 92%) as yellow solid. ^{1}H NMR (600 MHz, $CDCl_3$) δ 8.57 (d, J = 1.3 Hz, 2H), 8.18 (dd, J = 8.4, 1.5 Hz, 2H), 8.08 (s, 2H), 7.76 (d, J = 8.4 Hz, 2H), 3.08 (d, J = 7.5 Hz, 4H), 1.83 (quint, J = 7.5 Hz, 4H), 1.48 – 1.40 (m, 8H), 0.96 (t, J = 7.1 Hz, 6H). ^{13}C NMR (151 MHz, $CDCl_3$) δ 199.5, 143.2, 140.8, 132.1, 129.5, 128.2, 123.9, 123.4, 119.8, 117.3, 112.2, 38.8, 31.8, 24.4, 22.8, 14.2. HRMS (ESI): m/z calculated for $C_{30}H_{31}BrNO_2^+$ $[M+H]^+$ 516.1533, found 516.1533.

2-Bromo-5,11-dihexylindolo[3,2,1-*jk*]carbazole (2c). 450 ml anhydrous Et_2O were added to a dry three-necked flask, flushed with argon and cooled to 5 °C with ice/water. Under argon counterflow $AlCl_3$ (6.73 g, 50.5 mmol) and $LiAlH_4$ (1.91 g, 50.5 mmol) were added in portions. Subsequently, **2b** (6.20 g, 12.0 mmol) was dissolved in 100 ml anhydrous CH_2Cl_2 and added dropwise to the mixture. The reaction was slowly warmed to room temperature and stirred overnight. After quenching with 100 ml ethylacetate, the reaction mixture was filtered over celite and washed with CH_2Cl_2. After evaporation of the solvent, the crude product was flashed over silica (light petroleum/CH_2Cl_2) yielding **2c** (5.08 g, 10.40 mmol, 87%) as off-white solid. ^{1}H NMR (600 MHz, $CDCl_3$) δ 8.07 (s, 2H), 7.83 (d, J = 1.1 Hz, 2H), 7.70 (d, J = 8.2 Hz, 2H), 7.35 (dd, J = 8.2, 1.6 Hz, 2H), 2.79 (t, J = 7.7 Hz, 4H), 1.73 (p, J = 7.6 Hz, 4H),

1.43 – 1.32 (m, 12H), 0.91 (t, J = 7.1 Hz, 6H). ^{13}C NMR (151 MHz, $CDCl_3$) δ 142.6, 137.4, 136.8, 129.3, 127.9 123.1, 122.2, 119.8, 115.5, 111.8, 36.2, 32.2, 31.9, 29.1, 22.8, 14.3. HRMS (ESI): m/z calculated for $C_{30}H_{35}BrN^+$ $[M+H]^+$ 488.1947, found 488.1941.

General procedure for Miyaura Borylation towards boronic acid esters (GP3)[41]

A glass vial was charged with the corresponding brominated precursor (1.00 eq.), bis(pinacolato)diboron ($Bpin_2$) (1.20 eq.), KOAc (2.50 eq.) and $PdCl_2(dppf)*CH_2Cl_2$ (0.02 eq.) and flushed with argon. After addition of degassed DMF (2.5 ml/mmol) the reaction mixture was stirred at 100 °C until full conversion. The reaction was cooled to room temperature, poured into water and repeatedly extracted with CH_2Cl_2. The combined organic phases were dried over anhydrous Na_2SO_4 and concentrated under reduced pressure.

5,11-Bis(1,1-dimethylethyl)-2-(4,4,5,5-tetramethyl-1,3,2-dioxaborolan-2-yl)indolo[3,2,1-*jk*]carbazole (3a). The compound was prepared according to GP3 starting from **2a** (3.05 g, 7.05 mmol), $Bpin_2$ (2.15 g, 8.47 mmol), KOAc (1.72 g, 17.52 mmol) and $PdCl_2(dppf)*CH_2Cl_2$ (0.15 mmol). The crude product was purified by column chromatography (light petroleum/CH_2Cl_2, 10% - 35%) yielding **3a** (2.35 g, 4.90 mmol, 70%) as white solid. ^{1}H NMR (600 MHz, $CDCl_3$) δ 8.57 (s, 2H), 8.19 (d, J = 1.6 Hz, 2H), 7.81 (d, J = 8.4 Hz, 2H), 7.60 (dd, J = 8.4, 2.0 Hz, 2H), 1.47 (s, 18H), 1.45 (s, 12H). ^{13}C NMR (151 MHz, $CDCl_3$) δ 146.9, 145.0, 137.1, 129.9, 126.2, 124.3, 120.1, 118.7, 111.5, 83.9, 35.0, 32.0, 25.2 (C-B not detected). HRMS (ESI): m/z calculated for $C_{32}H_{39}BNO_2^+$ $[M+H]^+$ 480.3068, found 480.3074.

3,6-Dihexyl-9-(4-(4,4,5,5-tetramethyl-1,3,2-dioxaborolan-2-yl)phenyl)-9*H*-carbazole (6b). The compound was prepared according to GP3 starting from **5b** (2.14 g, 4.36 mmol), $Bpin_2$ (1.34 g, 5.28 mmol), KOAc (1.09 g, 10.90 mmol) and $PdCl_2(dppf)*CH_2Cl_2$ (71 mg, 0.09 mmol). The crude product was purified by column chromatography (light petroleum/CH_2Cl_2, 10% - 25%) yielding **6b** (1.52 g, 2.83 mmol, 65%) as colorless oil. ^{1}H NMR (600 MHz, CD_2Cl_2) δ 8.00 (d, J = 8.3 Hz, 2H), 7.92 (d, J = 1.2 Hz, 2H), 7.59 (d, J = 8.3 Hz, 2H), 7.37 (d, J = 8.3 Hz, 2H), 7.23 (dd, J = 8.4, 1.6 Hz, 2H), 2.79 (t, J = 7.7 Hz, 4H), 1.72 (quint, J = 7.6 Hz, 4H), 1.42 – 1.32 (m, 12H), 1.39 (s, 12H), 0.91 (t, J = 6.7, 6.3 Hz, 6H). ^{13}C NMR (151 MHz, CD_2Cl_2) δ 141.3, 139.7, 136.7, 135.4, 127.2, 126.2, 124.1, 120.0, 110.0, 84.6, 36.5, 32.9, 32.4, 29.6, 25.3, 23.3, 14.5 (C-B not detected). HRMS (ESI): m/z calculated for $C_{36}H_{49}BNO_2^+$ $[M+H]^+$ 538.3851, found 538.3853.

5,11-Dihexyl-2-(4,4,5,5-tetramethyl-1,3,2-dioxaborolan-2-yl)indolo[3,2,1-*jk*]carbazole (3b). The compound was prepared according to GP3 starting from **2c** (2.44 g, 5.03 mmol), $Bpin_2$ (1.53 g, 6.03 mmol), KOAc (1.24 g, 12.63 mmol) and $PdCl_2(dppf)*CH_2Cl_2$ (83 mg, 0.10 mmol). The crude product was purified by column chromatography (light petroleum/CH_2Cl_2, 15% - 25%) yielding **3b** (1.93 g, 3.59

mmol, 71%) as colorless oil, which crystallized after several days. ^{1}H NMR (600 MHz, $CDCl_3$) δ 8.54 (s, 2H), 7.94 (d, J = 1.3 Hz, 2H), 7.78 (d, J = 8.1 Hz, 2H), 7.36 (dd, J = 8.2, 1.6 Hz, 2H), 2.80 (t, J = 7.7 Hz, 4H), 1.73 (quint, J = 7.5 Hz, 4H), 1.45 (s, 12H), 1.42 – 1.32 (m, 12H), 0.90 (t, J = 6.8 Hz, 6H). ^{13}C NMR (151 MHz, $CDCl_3$) δ 146.6, 137.4, 136.6, 130.1, 127.2, 126.3, 123.1, 118.4, 111.8, 83.9, 36.2, 32.2, 31.9, 29.1, 25.2, 22.8, 14.3 (C-B not detected). HRMS (ESI): m/z calculated for $C_{36}H_{47}BNO_2^+$ $[M+H]^+$ 536.3694, found 536.3697.

General procedure for the solvent free Ullmann reaction (GP1)

Alkylated 2-bromoindolocarbazole (1.00 eq.), alkylated carbazole (1.50 eq.), K_2CO_3 (2.00 eq.) and $CuSO_4$*$5H_2O$ (0.10 eq.) were added to a glass vial stirred and at 230 °C in a heating block until full conversion according to TLC. After cooling to room temperature, the residue was dissolved in water and CH_2Cl_2. The phases were separated, and the aqueous phase extracted with CH_2Cl_2. The combined organic phases were dried over anhydrous Na_2SO_4 and concentrated under reduced pressure.

General procedure for the Suzuki coupling (GP2)

Alkylated 2-bromoindolocarbazole (1.00 eq.) and the corresponding boronic acid ester (1.25 eq.) were added to a three-neck flask and flushed with argon. Under argon counterflow $Pd(PPh_3)_4$ (5 mol%) was added. After addition of argon degassed anhydrous THF (20 ml/mmol) and aqueous K_2CO_3 (2.50 eq., 2M solution) the reaction was refluxed until full conversion according to TLC. After cooling to room temperature, the mixture was poured into water and extracted repeatedly with CH_2Cl_2. The combined organic phases were dried over anhydrous Na_2SO_4 and concentrated under reduced pressure.

5,11-Bis(1,1-dimethylethyl)-2-(3,6-bis(1,1-dimethylethyl)-9*H*-carbazol-9-yl)indolo[3,2,1-*jk*]carbazole (tBuICzCz). The compound was prepared according to GP1 starting from **2a** (1.30 g, 3.00 mmol), **4a** (1.26 g, 4.51 mmol), K_2CO_3 (0.83 g, 6.00 mmol) and $CuSO_4$*$5H_2O$ (75 mg, 0.30 mmol). Purification by column chromatography (light petroleum/CH_2Cl_2, 5% - 25%) gave **tBuICzCz** (1.45 g, 2.29 mmol, 77%) as white solid. ^{1}H NMR (600 MHz, $CDCl_3$) δ 8.23 (d, J = 1.5 Hz, 2H), 8.17 (s, 2H), 8.14 (d, J = 1.6 Hz, 2H), 7.88 (d, J = 8.5 Hz, 2H), 7.67 (dd, J = 8.5, 1.8 Hz, 2H), 7.49 (dd, J = 8.6, 1.8 Hz, 2H), 7.35 (d, J = 8.6 Hz, 2H), 1.51 (s, 18H), 1.48 (s, 18H). ^{13}C NMR (151 MHz, $CDCl_3$) δ 145.2, 143.5, 142.6, 141.0, 137.5, 133.1, 129.7, 125.0, 123.7, 123.1, 120.2, 119.4, 119.4, 116.3, 111.8, 109.4, 35.0, 34.9, 32.2, 32.0. HRMS (ESI): m/z calculated for $C_{46}H_{50}N_2^+$ $[M]^+$ 630.3969, found 630.3962.

2-(3,6-Dihexyl-9*H*-carbazol-9-yl)-5,11-dihexylindolo[3,2,1-*jk*]carbazole (HexICzCz). The compound was prepared according to GP1 starting from **2c** (1.47 g, 3.01 mmol), **4b** (1.52 g, 4.53 mmol), K_2CO_3 (833 mg, 6.03 mmol) and $CuSO_4$*$5H_2O$ (75 mg, 0.30 mmol). Purification by column chromatography (light petroleum/CH_2Cl_2, 1% - 2%) gave **HexICzCz** (1.75 g, 2.35 mmol, 78%) as yellow oil that crystallized after several days. ^{1}H NMR (600 MHz, CD_2Cl_2) δ 8.14 (s, 2H), 7.99 (s, 2H), 7.94 (s, 2H), 7.86 (d, J = 8.3

Hz, 2H), 7.44 (dd, J = 8.3, 1.5 Hz, 2H), 7.29 (d, J = 8.3 Hz, 2H), 7.23 (dd, J = 8.4, 1.5 Hz, 2H), 2.85 – 2.78 (m, 8H), 1.78 – 1.69 (m, 8H), 1.38 (d, J = 70.2 Hz, 24H), 0.94 – 0.88 (m, 12H). ^{13}C NMR (151 MHz, CD_2Cl_2) δ 143.7, 141.6, 138.1, 137.4, 134.8, 133.5, 130.2, 128.4, 127.1, 123.6, 123.6, 120.0, 119.9, 119.5, 112.4, 110.0, 36.6, 36.5, 33.0, 32.7, 32.4, 32.3, 29.7, 29.6, 23.3, 23.2, 14.5, 14.5. HRMS (ESI): m/z calculated for $C_{54}H_{66}N_2^+$ $[M]^+$ 742.5221, found 742.5220.

5,11-Bis(1,1-dimethylethyl)-2-(4-(3,6-bis(1,1-dimethylethyl)-9*H*-carbazol-9-yl)phenyl)indolo[3,2,1-*jk*]carbazole (tBuICzPCz). The compound was prepared according to GP2 starting from **2a** (1.08 g, 2.50 mmol), **6a** (1.50 g, 3.12 mmol), $Pd(PPh_3)_4$ (146 mg, 0.13 mmol) and K_2CO_3 (871 mg, 6.30 mmol, in 3.2 ml H_2O). Purification by column chromatography (light petroleum/CH_2Cl_2, 5% - 8%) gave **tBuICzPCz** (1.31 g, 1.85 mmol, 74%) as white solid. ^{1}H NMR (600 MHz, $CDCl_3$) δ 8.37 (s, 2H), 8.24 (d, J = 1.7 Hz, 2H), 8.18 (d, J = 1.5 Hz, 2H), 8.00 (d, J = 8.3 Hz, 2H), 7.85 (d, J = 8.5 Hz, 2H), 7.70 (d, J = 8.3 Hz, 2H), 7.65 (dd, J = 8.5, 1.9 Hz, 2H), 7.52 (dd, J = 8.6, 1.8 Hz, 2H), 7.48 (d, J = 8.6 Hz, 2H), 1.50 (s, 18H), 1.50 (s, 18H). ^{13}C NMR (151 MHz, $CDCl_3$) δ 145.0, 144.6, 142.9, 142.4, 139.5, 137.4, 136.7, 136.5, 129.9, 129.6, 127.1, 124.6, 123.8, 123.5, 120.0, 119.2, 119.1, 116.4, 111.7, 109.5, 35.1, 34.9, 32.2, 32.0. HRMS (ESI): m/z calculated for $C_{52}H_{54}N_2^+$ $[M]^+$ 706.4282, found 706.4280.

2-(4-(3,6-Dihexyl-9*H*-carbazol-9-yl)phenyl)-5,11-dihexylindolo[3,2,1-*jk*]carbazole (HexICzPCz). The compound was prepared according to GP2 starting from **2c** (1.22 g, 2.50 mmol), **6b** (1.41 g, 2.62 mmol), $Pd(PPh_3)_4$ (145 mg, 0.13 mmol) and K_2CO_3 (866 mg, 6.27 mmol, in 3.2 ml H_2O). Purification by column chromatography (light petroleum/CH_2Cl_2 3% - 10%) gave **HexICzPCz** (1.08 g, 1.32 mmol, 53%) as off-white solid. ^{1}H NMR (600 MHz, CD_2Cl_2) δ 8.32 (s, 2H), 8.03 (s, 2H), 7.99 (d, J = 8.3 Hz, 2H), 7.96 (s, 2H), 7.81 (d, J = 8.2 Hz, 2H), 7.71 (d, J = 8.3 Hz, 2H), 7.46 (d, J = 8.3 Hz, 2H), 7.42 (d, J = 8.2 Hz, 2H), 7.28 (d, J = 8.4 Hz, 2H), 2.87 – 2.79 (m, 8H), 1.81 – 1.71 (m, 8H), 1.47 – 1.32 (m, 24H), 0.92 (t, J = 6.7 Hz, 12H). ^{13}C NMR (151 MHz, CD_2Cl_2) δ 144.7, 142.7, 140.1, 138.0, 137.2, 137.2, 136.8, 135.1, 130.4, 129.9, 128.0, 127.5, 127.1, 124.0, 123.4, 120.0, 119.4, 119.3, 112.3, 110.0, 36.6, 36.5, 32.9, 32.7, 32.4, 32.4, 29.7, 29.6, 23.3, 23.3, 14.5, 14.5.. HRMS (ESI): m/z calculated for $C_{60}H_{70}N_2^+$ $[M]^+$ 818.5534, found 818.5537.

5,5',11,11'-Tetra-bis(1,1-dimethylethyl)-2,2'-biindolo[3,2,1-*jk*]carbazole (tBuICzICz). The compound was prepared according to GP2 starting from **2a** (1.08 g, 2.50 mmol), **3a** (1.50 g, 3.13 mmol), $Pd(PPh_3)_4$ (146 mg, 0.13 mmol) and K_2CO_3 (869 mg, 6.29 mmol, in 3.2 ml H_2O). Purification by column chromatography (light petroleum/CH_2Cl_2 5% - 25%) gave **tBuICzICz** (0.62 g, 0.88 mmol, 35%) as white solid. ^{1}H NMR (600 MHz, $CDCl_3$) δ 8.45 (s, 4H), 8.25 (s, 4H), 7.86 (d, J = 8.5 Hz, 4H), 7.64 (d, J = 10.4 Hz, 4H), 1.50 (s, 36H). ^{13}C NMR (151 MHz, $CDCl_3$) δ 144.8, 144.2, 139.8, 137.4, 130.1, 124.4, 120.3, 120.0, 119.0, 111.6, 35.1, 32.1. HRMS (ESI): m/z calculated for $C_{52}H_{52}N_2^+$ $[M]^+$ 704.4125, found 704.4128.

5,5',11,11'-Tetrahexyl-2,2'-biindolo[3,2,1-*jk*]carbazole (HexICzICz). The compound was prepared according to GP2 starting from **2c** (1.22 g, 2.50 mmol), **3b** (1.49 g, 2.78 mmol), $Pd(PPh_3)_4$ (147 mg, 0.13 mmol) and K_2CO_3 (866 mg, 6.27 mmol, in 3.2 ml H_2O). Purification by column chromatography (light petroleum/CH_2Cl_2 5% - 15%) gave **HexICzICz** (0.89 g, 1.09 mmol, 44%) as off-white solid. ^{1}H NMR (600 MHz, $CDCl_3$) δ 8.37 (s, 4H), 8.01 (s, 4H), 7.81 (d, J = 8.2 Hz, 4H), 7.39 (d, J = 8.2 Hz, 4H), 2.83 (t, J = 7.7 Hz, 8H), 1.76 (p, J = 7.6 Hz, 8H), 1.46 – 1.32 (m, 24H), 0.91 (t, J = 7.0 Hz, 12H). ^{13}C NMR (151 MHz, $CDCl_3$) δ 144.0, 139.7, 137.7, 136.4, 130.3, 127.3, 123.0, 120.3, 118.7, 111.9, 36.3, 32.3, 32.0, 29.2, 22.8, 14.3. HRMS (ESI): m/z calculated for $C_{60}H_{68}N_2^+$ $[M]^+$ 816.5377, found 816.5376.

ACHNOWLEDGEMENT

T.K., J.F., and P.K. gratefully acknowledge financial support by the Austrian Science Fund (FWF) (grant No. I 2589-N34). Charlie Lim is acknowledged for supporting the experimental work. Anh Dung Tran is acknowledged for performing the STA measurements.

SUPPORTING INFORMATION

Description of the experimental setup of the solubility study, cyclic voltammograms, DSC-/STA-curves, ^{1}H and ^{13}C NMR spectra of the materials, as well as external quantum efficiency – luminance curves and photoluminescence spectra of the devices can be found in the supporting information.

REFERENCES

[1] P. S. Vincett, W. A. Barlow, R. A. Hann, G. G. Roberts, *Thin Solid Films* **1982**, *94*, 171-183.

[2] C. W. Tang, S. A. VanSlyke, *Applied Physics Letters* **1987**, *51*, 913-915.

[3] J. H. Burroughes, D. D. C. Bradley, A. R. Brown, R. N. Marks, K. Mackay, R. H. Friend, P. L. Burns, A. B. Holmes, *Nature* **1990**, *347*, 539-541.

[4] M. A. Baldo, D. F. O'Brien, Y. You, A. Shoustikov, S. Sibley, M. E. Thompson, S. R. Forrest, *Nature* **1998**, *395*, 151-154.

[5] C. Adachi, M. A. Baldo, M. E. Thompson, S. R. Forrest, *Journal of Applied Physics* **2001**, *90*, 5048-5051.

[6] A. Endo, M. Ogasawara, A. Takahashi, D. Yokoyama, Y. Kato, C. Adachi, *Advanced Materials* **2009**, *21*, 4802-4806.

[7] A. Endo, K. Sato, K. Yoshimura, T. Kai, A. Kawada, H. Miyazaki, C. Adachi, *Applied Physics Letters* **2011**, *98*, 083302.

[8] P. Kautny, D. Lumpi, Y. Wang, A. Tissot, J. Bintinger, E. Horkel, B. Stöger, C. Hametner, H. Hagemann, D. Ma, J. Fröhlich, *Journal of Materials Chemistry C* **2014**, *2*, 2069-2081.

[9] P. Kautny, Z. Wu, J. Eichelter, E. Horkel, B. Stöger, J. Chen, D. Ma, J. Fröhlich, D. Lumpi, *Organic Electronics* **2016**, *34*, 237-245.

[10] Y. Im, S. H. Han, J. Y. Lee, *Journal of Industrial and Engineering Chemistry* **2018**, *66*, 381-386.

[11] J.-A. Seo, Y. Im, S. H. Han, C. W. Lee, J. Y. Lee, *ACS Applied Materials & Interfaces* **2017**, *9*, 37864-37872.

[12] V. V. Patil, K. H. Lee, J. Y. Lee, *Dyes and Pigments* **2019**, 108070.

[13] D. Bader, J. Fröhlich, P. Kautny, *The Journal of Organic Chemistry* **2019**, *85*, 3865-3871.

[14] T. Kader, B. Stöger, J. Fröhlich, P. Kautny, *Chemistry – A European Journal* **2019**, *25*, 4412-4425.

[15] Y. Im, S. H. Han, J. Y. Lee, *Journal of Materials Chemistry C* **2018**, *6*, 5012-5017.

[16] H. G. Dunlop, S. H. Tucker, *Journal of the Chemical Society* **1939**, 1945-1956.

[17] S. I. Wharton, J. B. Henry, H. McNab, A. R. Mount, *Chemistry – A European Journal* **2009**, *15*, 5482-5490.

[18] J. B. Henry, S. I. Wharton, E. R. Wood, H. McNab, A. R. Mount, *The Journal of Physical Chemistry A* **2011**, *115*, 5435-5442.

[19] J. Lv, Q. Liu, J. Tang, F. Perdih, K. Kranjc, *Tetrahedron Letters* **2012**, *53*, 5248-5252.

[20] A. W. Jones, M.-L. Louillat-Habermeyer, F. W. Patureau, *Advanced Synthesis & Catalysis* **2015**, *357*, 945-949.

[21] C. Luo, W. Bi, S. Deng, J. Zhang, S. Chen, B. Li, Q. Liu, H. Peng, J. Chu, *The Journal of Physical Chemistry C* **2014**, *118*, 14211-14217.

[22] W. Cao, M. Fang, Z. Chai, H. Xu, T. Duan, Z. Li, X. Chen, J. Qin, H. Han, *RSC Advances* **2015**, *5*, 32967-32975.

[23] F. Hinkel, Y. M. Kim, Y. Zagraniarsky, F. Schlütter, D. Andrienko, K. Müllen, F. Laquai, *The Journal of Chemical Physics* **2018**, *148*, 044703.

[24] X.-J. Ma, X.-D. Zhu, K.-L. Wang, F. Igbari, Y. Yuan, Y. Zhang, C.-H. Gao, Z.-Q. Jiang, Z.-K. Wang, L.-S. Liao, *Nano Energy* **2019**, *63*, 103865.

[25] Y. Im, S. H. Han, J. Y. Lee, *Organic Electronics* **2018**.

[26] C. Zhao, T. Schwartz, B. Stöger, F. J. White, J. Chen, D. Ma, J. Fröhlich, P. Kautny, *Journal of Materials Chemistry C* **2018**, *6*, 9914-9924.

[27] X.-H. Zheng, J.-W. Zhao, T.-T. Huang, X. Chen, C. Cao, G.-X. Yang, Z.-H. Lin, Q.-X. Tong, S.-L. Tao, D. Liu, *ChemElectroChem* **2019**, *n/a*.

[28] Y. Im, S. H. Han, J. Y. Lee, *Dyes and Pigments* **2019**, *164*, 233-236.

[29] B. Holzer, J. Bintinger, D. Lumpi, C. Choi, Y. Kim, B. Stöger, C. Hametner, M. Marchetti-Deschmann, F. Plasser, E. Horkel, I. Kymissis, J. Fröhlich, *ChemPhysChem* **2017**, *18*, 549-563.

[30] V. V. Patil, K. H. Lee, J. Y. Lee, *Journal of Materials Chemistry C* **2019**, *7*, 14301-14305.

[31] C. Niebel, V. Lokshin, A. Ben-Asuly, W. Marine, A. Karapetyan, V. Khodorkovsky, *New Journal of Chemistry* **2010**, *34*, 1243-1246.
[32] M. Rivoal, L. Bekere, D. Gachet, V. Lokshin, W. Marine, V. Khodorkovsky, *Tetrahedron* **2013**, *69*, 3302-3307.
[33] R. K. Konidena, K. H. Lee, J. Y. Lee, W. P. Hong, *Journal of Materials Chemistry C* **2019**, *7*, 8037-8044.
[34] T. Taniguchi, Y. Itai, Y. Nishii, N. Tohnai, M. Miura, *Chemistry Letters* **2019**, *48*, 1160-1163.
[35] K. S. Yook, J. Y. Lee, *Advanced Materials* **2014**, *26*, 4218-4233.
[36] L. Duan, L. Hou, T.-W. Lee, J. Qiao, D. Zhang, G. Dong, L. Wang, Y. Qiu, *Journal of Materials Chemistry* **2010**, *20*, 6392-6407.
[37] Y. Zou, S. Gong, G. Xie, C. Yang, *Advanced Optical Materials* **2018**, *6*, 1800568.
[38] Y. Liu, M. Nishiura, Y. Wang, Z. Hou, *Journal of the American Chemical Society* **2006**, *128*, 5592-5593.
[39] X.-Y. Wang, D.-C. Yang, F.-D. Zhuang, J.-J. Liu, J.-Y. Wang, J. Pei, *Chemistry – A European Journal* **2015**, *21*, 8867-8873.
[40] L. Wang, E. Ji, N. Liu, B. Dai, *Synthesis* **2016**, *48*, 737-750.
[41] M. Yu, S. Wang, S. Shao, J. Ding, L. Wang, X. Jing, F. Wang, *Journal of Materials Chemistry C* **2015**, *3*, 861-869.
[42] J. F. Ambrose, R. F. Nelson, *Journal of the Electrochemical Society* **1968**, *115*, 1159-1164.
[43] J. F. Ambrose, L. L. Carpenter, R. F. Nelson, *Journal of the Electrochemical Society* **1975**, *122*, 876-894.